NASA TM X-73,113 FAA-RD-75-206

WAKE VORTEX ENCOUNTER HAZARD CRITERIA FOR TWO AIRCRAFT CLASSES

Robert I. Sammonds and Glen W. Stinnett, Jr.
Ames Research Center
Moffett Field, California 94035

William E. Larsen
Federal Aviation Administration
Washington, D. C. 20591

June 1976

1 Report No. NASA TM X-73,113 FAA-RD-75-206	2. Government Accession No.	3 Recipient's Catalog No.
4. Title and Subtitle WAKE VORTEX ENCOUNTER HAZARD CRITERIA FOR TWO AIRCRAFT CLASSES		5. Report Date 6. Performing Organization Code
7. Author(s) Robert I. Sammonds,* Glen W. Stinnett, Jr.,* and William E. Larsen**		8. Performing Organization Report No A-6493
9. Performing Organization Name and Address *Ames Research Center, Moffett Field, Calif. 94035 **Federal Aviation Administration, Washington, D. C. 20591		10. Work Unit No. 505-08-22 11 Contract or Grant No.
12. Sponsoring Agency Name and Address National Aeronautics and Space Administration Washington, D. C. 20546		13. Type of Report and Period Covered Technical Memorandum 14. Sponsoring Agency Code
15. Supplementary Notes		

16. Abstract

Development of techniques for reducing the current longitudinal separations (4-6 mi) required to avoid hazardous encounters with trailing wake vortices of preceding aircraft during approach and landings is a goal of the Federal Aviation Administration. One technique under consideration is the implementation of a wake vortex avoidance system that would utilize criteria relating the hazard of the encounter to the response of the encountering aircraft to adjust spacings to avoid hazardous encounters.

An investigation was conducted using a piloted, motion-base simulator (NASA-Ames Flight Simulator for Advanced Aircraft, FSAA) to determine wake vortex hazard criteria for two classes of jet transport aircraft. These aircraft, the Learjet 23 and the Boeing 707/720, represented a light business jet and a large multiengine jet transport, respectively. The hazard boundaries were determined in terms of the maximum bank angle due to the vortex encounter, a parameter shown in a previous investigation to provide the best correlation with the pilot assessment of the hazard.

Upsets as small as 7° in bank angle were considered to be hazardous at breakout altitude (200 ft (61.0 m)) for IFR and at 50 ft (15.2 m) for VFR for both aircraft classes.

Proximity to the ground was the primary reason for a hazardous rating. This was reflected in the reduction in the maximum bank angle at the hazard boundary and in more consistent ratings as altitude was decreased.

17. Key Words (Suggested by Author(s))	18. Distribution Statement
Wake vortex Wake vortex encounters Wake vortex hazard criteria Wake vortex encounter simulation	Unlimited STAR Category - 03

19. Security Classif. (of this report)	20. Security Classif. (of this page)	21. No. of Pages	22. Price*
Unclassified	Unclassified	40	$3.75

*For sale by the National Technical Information Service, Springfield, Virginia 22161

SYMBOLS

a_x, a_y, a_z	accelerations along the x, y, z aircraft axes
IFR	instrument flight rules
p,q,r	angular velocities about x, y, z aircraft axes
$\dot{p}, \dot{q}, \dot{r}$	angular accelerations about x, y, z aircraft axes
FAA	Federal Aviation Administration
VFR	visual flight rules
x,y,z	cartesian coordinates and distances along these axes
θ	pitch attitude
ϕ	bank angle
ψ	heading angle
(ψ, θ, ϕ)	Euler angles relating airplane wind axes to the vortex axes

WAKE VORTEX ENCOUNTER HAZARD CRITERIA FOR TWO AIRCRAFT CLASSES

Robert I. Sammonds, Glen W. Stinnett, Jr., and William E. Larsen*

Ames Research Center

SUMMARY

Development of techniques for reducing the current longitudinal separations (4-6 mi) required to avoid hazardous encounters with trailing wake vortices of preceding aircraft during approach and landings is a goal of the Federal Aviation Administration. One technique under consideration is the implementation of a wake vortex avoidance system that would utilize criteria relating the hazard of the encounter to the response of the encountering aircraft to adjust spacings to avoid hazardous encounters.

An investigation was conducted using a piloted, motion-base simulator (NASA-Ames Flight Simulator for Advanced Aircraft, FSAA) to determine wake vortex hazard criteria for two classes of jet transport aircraft. These aircraft, the Learjet 23 and the Boeing 707/720, represented a light business jet and a large multiengine jet transport, respectively. The hazard boundaries were determined in terms of the maximum bank angle due to the vortex encounter, a parameter shown in a previous investigation to provide the best correlation with the pilot assessment of the hazard.

Upsets as small as 7° in bank angle were considered to be hazardous at breakout altitude (200 ft (61.0 m)) for IFR and at 50 ft (15.2 m) for VFR for both aircraft classes.

Proximity to the ground was the primary reason for a hazardous rating. This was reflected in the reduction in the maximum bank angle at the hazard boundary and in more consistent ratings as altitude was decreased.

INTRODUCTION

Increased traffic at major airports in this country has led to a program by the Federal Aviation Administration to develop an "Updated Third Generation" air traffic control system designed to increase airport capacity and improve safety (ref. 1). The success of this system is dependent upon development of techniques for reducing the current longitudinal separations (4-6 mi) required to avoid the hazard from trailing wake vortices, particularly from large aircraft during approach and landing (refs. 2-7). One technique under consideration is the implementation of a wake vortex avoidance system which would rely on information from ground-based measurements (refs. 3, 6, and 7) to adjust spacings to avoid hazardous encounters when it is predicted that a vortex from preceding aircraft would lie in the approach

*Federal Aviation Administration, Washington, D. C. 20591.

path. The goal of this system is to reduce longitudinal separations of aircraft to 2 mi (ref. 8).

Determination of criteria relating the hazard of the encounter to the response of the encountering aircraft was the purpose of a joint NASA/FAA research program conducted at Ames Research Center using the piloted six-degrees-of-freedom (6-DOF) motion Flight Simulator for Advanced Aircraft (FSAA). These criteria were determined from the subjective assessment, by a number of pilots, of numerous simulated wake vortex encounters during a landing approach task. A preliminary investigation, reference 9, validated the ability of simulators to produce realistic encounters, established that pilot opinion of hazard correlates best with maximum bank angle, and provided data for development of a pilot model for use in unmanned simulations.

The present investigation was undertaken to establish hazard criteria for two classes of aircraft having different inertia and response characteristics and to provide additional data for development of a pilot model. The two classes of aircraft of interest are represented by a light general aviation twin-jet (Learjet) and a large four-jet transport (Boeing 707/720). The pilot model was developed separately by Systems Technology, Inc. under contract (ref. 10). This contractor was also responsible for development of the simulation models for both aircraft types.

SIMULATION

Description of the Simulator

The investigation was conducted on the NASA-Ames Research Center FSAA shown in figure 1. Details pertinent to the present investigation are presented below.

Motion capabilities— The motion capability of the FSAA is given in table 1. The motion logic, including washout, residual tilt, limiting circuits, and cross-coupling terms, is discussed briefly in appendix A. Bode plots of frequency response for the basic simulator are also presented in appendix A.

Cab details— The simulator (fig. 1) was equipped with a three-man jet transport cab with the instrumentation required for VFR and IFR landing approach tasks as listed in table 2 and shown in figure 2. The cab was equipped with throttle, gear, and flap controls to allow abort, clean-up, and go-around. The cab was also equipped with hydraulically actuated control loaders for the wheel, column, and rudder pedals. These hydraulic loaders were programmed to give the desired dynamic force-feel characteristics of each aircraft during the landing approach phase of flight.

Visual and aural cues-- The pilot in the cab was provided visual and aural cues as well as the motion cues. The visual cues consisted of a landing approach scene displayed on a collimated color TV monitor mounted above the instrument panel. The visual scene was generated by a computer-driven 6-DOF

TV camera that duplicated the aircraft motion with respect to the landing approach scene. Although the simulator motion was restricted by physical limitations and washout terms, the visual scene was not subject to these same restraints. The frequency response characteristics of the visual system are given in appendix A.

The aural cues consisted of engine noise modulated by computed engine rpm and were introduced through stereo speakers located in the cab.

Modeling

Conventional simulation math models to represent the Gates/Learjet Model 23 and the Boeing 707/720 were developed. The forces and moments caused by encounter with the vortex were simply superimposed upon those computed for this conventional math model. Representation of the vortex encounter requires a mathematical model of the vortex, and its interaction with the encountering aircraft. In addition, the simulation required special computations to ensure that repeatable encounters were obtained. Finally, turbulence was introduced that was modeled so that pilot describing function information could be derived from the measured pilot response. These modeling efforts for the wake vortex encounter simulation are described briefly in the following paragraphs. A more detailed description of the modeling used for the vortex and the Boeing 707/720 is given in reference 11.

Aircraft model— The aerodynamic models used during this simulation represent the Gates/Learjet Model 23 and the Boeing 707/720; they include approach and takeoff configurations. The model defines the aircraft control system variables and provides for clean-up and go-around following an aborted approach.

Vortex model— The vortex model was defined by a pair of two-dimensional vortices. The parameters that characterized the flow field in each case were vortex spacing, core diameter, and circulation strength. The tangential velocity from each vortex was calculated from the following equation, and the resultant velocity at a given point was computed in the manner described in references 11 and 12.

$$\left|V_T\right| = \frac{\Gamma_o}{2\pi r}\left[1 - e^{-r^2/4\varepsilon\tau}\right] \tag{1}$$

where V_T is the tangential vortex velocity; Γ_o is the vortex strength (a function of the weight, speed, and wingspan of the generating airplane); $\varepsilon = 0.0002\ \Gamma_o$, which represents the vortex decay effect; τ is the age of the vortex; and r is the radial distance from the center of the vortex.

The tangential velocity out to a radius of 35 ft (10.67 m) was determined according to equation (1) and then decreased linearly to become 0 at a radius of 70 ft (21.34 m). The objective of this truncation of the flow field was to make it impossible for the pilot to sense the presence of the vortex at greater distances and preserve the characteristic suddenness of the upsets

observed in flight. For this program, only one core diameter was used (10 ft (3 m)) since it has been shown in reference 9 that small variations in core diameter have no particular effect on the upset. The vortex properties were chosen to obtain the desired upset magnitude. No attempts were made to duplicate values characteristic of any particular aircraft.

The axes of the two vortices from the generating airplane were assumed to be straight lines, and to be separated by 84 ft (25.6 m) and 150 ft (45.7 m) for the Learjet and Boeing simulations, respectively. These separation distances are typical of those for the Boeing 727 and 747, respectively, in the landing configuration.

Encounter geometry— The severity of a vortex upset depends not only on vortex strength, but also on the encounter conditions (i.e., how close the aircraft comes to the vortex core and the angle of the flight path relative to the vortex axis). These encounter conditions were specified in terms of a target point and an entry angle as shown in figure 3. The target point specifies how close the aircraft's initial velocity vector (aircraft C.G.) comes to the vortex core, and the entry angle specifies the attitude of the velocity vector relative to the vortex axis. To ensure that the aircraft's center of gravity would traverse the target point and obtain repeatable encounters, the vortex origin was translated and rotated in such a manner that the aircraft's center of gravity was always heading toward the target point regardless of aircraft motions. Just prior to reaching the target point, the vortex origin was frozen in inertial space. The location of the freeze point was selected close enough to the target point to ensure penetration regardless of pilot maneuvering. For the present simulation, the target point was always located at the center of the vortex core. A more detailed explanation of the encounter geometry and the technique for obtaining repeated encounters are given in reference 11.

Vortex-aircraft interaction model— The forces and moments due to the presence of the vortex flow field were calculated by strip theory using the methods shown in references 11 and 12. In brief, this procedure divides the wing, horizontal tail, and vertical tail into N-number of chordwise strips. (For this case, the wing was divided into 20 strips per semispan while the horizontal and vertical tails were each divided into 6 strips per panel for each aircraft.) The local velocity, angles of attack and sideslip, and forces and moments (referred to the airplane center of gravity) due to the vortex were calculated for each strip. These incremental forces and moments were summed and combined with estimated fuselage contributions to give the net forces and moments on the airplane due to the vortex.

Turbulence model— Turbulence was introduced to obtain the pilot response to a known disturbance for the development of pilot describing functions. The disturbances due to turbulence were generated by equivalent aileron and elevator inputs which were added to the pilot inputs. The equivalent aileron and elevator inputs were computed as follows:

$$\delta_j = \sum_{j=1}^{1} A_j \sin(\omega_j t + \phi_j) \qquad (2)$$

where the phase (ϕ_j) was randomly selected for each run, the frequencies (ω_j) were specified in terms of number of cycles over a given time period, and the amplitude (A_j) were specified in degrees of control surface (elevator and aileron). Numerical values of these variables are shown in table 3 where

$$\omega_j = \frac{2\pi N_j}{T_{run}} \tag{3}$$

and

$$T_{run} = 40 \text{ sec}$$

TEST PROGRAM

Task

The test program was limited to vortex encounters during landing approach. The piloting task was to fly either an IFR or VFR approach on a 3° glide slope with the aircraft trimmed on glide slope and localizer 3 mi out and at the proper airspeed. The pilot was instructed to continue the approach if possible but was given abort capability if desired (gear, flap, and engine control).

Hazard Evaluation

For each vortex encounter the pilot was asked to assess the hazard in terms of a rating scale developed for this simulation. This rating scale (fig. 4) required the pilot to decide whether or not an abort was necessary and, in the event of an abort, to rate the probability of an accident due to the upset. The pilot was instructed to base his evaluation only on the possibility of damage to the aircraft. Passenger comfort was not to be considered a factor. He was also instructed to consider ratings of A and B to be nonhazardous and ratings of C and D to be hazardous. This subjective assessment provided the only evaluation of the hazard posed by the encounter. A pilot questionnaire (fig. 5) was used to stimulate a response from the pilot and provide an insight into the reasons for the hazard ratings.

Test Procedure

Since the objective of this investigation was to determine a boundary that would separate the data into nonhazardous and potentially hazardous regions, it was desirable that most of the encounters be near the hazard boundary. This was accomplished by observing the position of the boundary as the test progressed and adjusting the vortex strength accordingly. Most encounters, therefore, were rated as either B or C according to the rating scale.

Data Acquisition

In addition to the pilot's assessment of the hazard, a number of response parameters such as bank angle, roll rate, altitude and control surface deflections, etc. were recorded on two 8-channel Brush recorders, a line printer, and a digital tape.

Test Conditions

The vortex strengths were modulated, as previously mentioned, to give the desired distributions of upset magnitudes for several encounter angles at nominal encounter altitudes of 100 ft (30.5 m), 200 ft (61.0 m), 350 ft (106.7 m), and 500 ft (152.4 m).

Encounters were made for two turbulence levels either into the right or left vortex with altitude, and encounter angle selected randomly. In some instances, an approach would be made without an encounter. This procedure precluded the pilot predicting when an encounter might occur, how severe it would be, and its precise nature.

The encounter angles used and their relationship to the vortices are shown in table 4.

RESULTS AND DISCUSSION

A simulator investigation was conducted to establish wake vortex encounter hazard boundaries for two widely different classes of jet transport aircraft. The test plan was formulated on the basis of an earlier investigation reported in reference 9. The primary purposes of this earlier investigation were to determine if wake vortex encounters could be simulated with sufficient realism to permit pilot assessment of the hazard and to define criteria in terms of aircraft response that provide the best correlation with pilot opinion. A tentative hazard boundary for a small business jet (Learjet-23) was defined during this investigation for VFR conditions.

The second investigation differed somewhat from the first in several respects. First, a different simulator was used which had greater lateral travel. This permitted not only improved fidelity of motion cues due to lateral acceleration, but also improved the fidelity of the roll acceleration cues. (See appendix A for description of simulator motion logic.) A second difference between the two simulations was in the scale used to rate the hazard due to the vortex encounter. In the first investigation, the data were correlated on the basis of pilot responses to the question "Did you consider the encounter to be hazardous?" For the second investigation, a rating scale was developed to delineate several levels of hazard due to a vortex encounter. This scale is shown in figure 4. It was made clear to all participating pilots (see appendix B for pilot résumés) that the boundary between hazardous and nonhazardous encounters lay between ratings B and C. As noted in the

section on test procedure, the vortex strength was varied during the course of the experiment to attempt to distribute the response so that most ratings would be either B or C. In presenting the results, it was found that there was no advantage in including all four ratings. Accordingly, all encounters are classified either as nonhazardous (A or B) or hazardous (C or D).

Data were obtained during the second investigation to complete the definition of the hazard boundary for a small business jet aircraft, as represented by the Learjet-23. The representation of this aircraft, however, was somewhat different for the two investigations as a result of the different emphasis placed on each experiment. Since the emphasis during the first investigation was placed on establishing that the encounters were comparable to those experienced by the pilots in flight, a similar aircraft model was required. This model thus specified that the yaw damper be engaged at all times. However, the emphasis during the second investigation was to establish hazard boundaries for the landing approach task. Standard operating procedure for landing approach requires the damper to be disengaged during the approach. Thus, the math model for the second investigation specified that the yaw damper be disengaged at all times.

Comparison of Results With First Investigation

The first investigation (ref. 9) established the maximum bank angle that occurred in response to the vortex as the aircraft response parameter that provided the best separation of the data into nonhazardous and possibly hazardous regions. This criterion was employed to determine the hazard boundaries on the basis of the data obtained during the second investigation.

Hazard assessments, restricted to three of the four pilots who participated in both investigations, are shown in figure 6. These three pilots were responsible for 90 percent of the data obtained during the first investigation and 50 percent of the data during the second investigation. On the basis of these results, a more conservative hazard boundary would be drawn from the present data (FSAA) than was indicated on the basis of the first investigation (ref. 9). However, this new boundary would encompass only four encounters rated as hazardous that lay outside of the boundary established from the first investigation.

It was noted from the results of the first investigation that the hazard boundary appeared to be representative of the opinion of all of the participating pilots in that each rated at least one encounter as hazardous that was close to it. An inspection of the data shown in figures 7-10 indicated that this unanimity did not exist during the second investigation. For instance, the results for VFR approaches for the Learjet (fig. 7) indicated a boundary more conservative than would be drawn on the basis of the data shown in figure 6. The difference in the two boundaries is the result of two encounters rated as hazardous by pilot D at nominal altitudes of 350 ft (106.7 m) and 500 ft (152.4 m). Similar situations are evident in other results for both VFR and IFR conditions.

Hazard Boundaries

Hazard boundaries have been drawn in figures 7-10 for altitudes from 50 ft (15.2 m) to 500 ft (152.4 m) for VFR conditions and from 200 ft (61.0 m) to 500 ft (152.4 m) for IFR conditions. These boundaries separate the data into two regions, one containing only nonhazardous encounters and the other containing both hazardous and nonhazardous encounters. Thus, these boundaries, as drawn, represent the most conservative rating of all the pilots even though it has been shown previously that the boundaries drawn for individual pilots vary considerably. It can also be seen from these data that the band of nonhazardous encounters included in the potentially hazardous region is more widespread at the higher altitudes than at the lower altitudes. Thus, in essence, this can be considered to be scatter in the data that reflects the latitude available to the pilot in making his subjective assessment of the hazard. A decrease in the amount of scatter thus represents a more conclusive assessment of the hazard.

For VFR flight conditions, both the maximum acceptable bank angle and the scatter in the data decreased markedly with decreasing altitude. For example, at an altitude of 100 ft (30.5 m), the boundaries shown in figures 7 and 8 show maximum acceptable bank angles of 6°-8° and a scatter of about 6°. At an altitude of 500 ft (152.4 m), however, the maximum acceptable bank angles increase to 20°-25°, depending on aircraft type, with the amount of scatter increasing to 25°-30°.

For IFR flight conditions, the maximum acceptable bank angle remains constant at altitudes above 350 ft (106.7 m) but decreases significantly at the lower altitudes. The scatter in the data is comparable to that obtained under VFR conditions for comparable altitudes.

The hazard boundaries shown in figures 7-10 are summarized in figure 11 for both the Learjet and the Boeing 707/720 for both VFR and IFR flight conditions. For VFR conditions, the hazard boundary is nearly the same for both aircraft at the lower altitude but diverges with increasing altitude. As might be expected, the hazard boundary for the larger aircraft is the more conservative. As noted previously, the hazard boundary, under IFR conditions, for both aircraft remained constant at about 10° for altitudes above 350 ft (106.7 m) but decreased to about 7° at the breakout altitude of 200 ft (61 m). The hazard boundary for IFR conditions is shown to be on the order of 50 percent of that for VFR conditions for the larger aircraft. For both VFR and IFR conditions, upsets as small as 7° in bank angle were considered hazardous at the lower altitudes.

The commentary by the pilots in response to the questionnaire shown in figure 5 was reviewed to reveal any consistent patterns that could be used to augment the results. The following observations are worthy of note:

1. In general, the upsets were felt to be quite realistic, particularly with regard to roll response.

2. In most cases, the encounters were easily distinguishable as being vortex generated in either smooth air or moderate turbulence. This is of

particular interest for the smaller upsets because the question arises as to whether a vortex encounter can be distinguished from upsets from normal atmospheric turbulence. It was determined from responses to the pilot questionnaire that, for maximum bank angles due to the vortex from 5° to 10°, 88 percent of the encounters in smooth air were recognized as being vortex generated. When moderate turbulence was present, the ability of the pilots to differentiate between upset type was reduced to 69 percent.

3. The primary reason for rating an encounter as hazardous was proximity to the ground at the time of the encounter or subsequent altitude loss as a result of the encounter. This is reflected in the reduction in the maximum bank angle at the hazard boundary and in the more consistent ratings as altitude is decreased.

4. Misalignment with the runway and/or glide slope was frequently cited as the reason for a hazardous rating due to the dangers involved in attempting to recover and reacquire the track. Misalignment on the approach generally resulted from an encounter that tossed the aircraft to one side or below the glide slope.

5. Disorientation associated with encounters under instrument conditions and sudden or violent upsets that startled the pilots were additional factors leading to hazardous ratings.

CONCLUDING REMARKS

Using piloted simulators, tentative boundaries separating nonhazardous and potentially hazardous wake vortex encounters during a landing approach task have been obtained for a light twin-jet (Learjet) and a large four-engine transport (Boeing 707/720) for both VFR and IFR flight conditions. For VFR conditions, boundaries for both were the same at the lower altitudes but diverged at the higher altitudes, becoming more conservative for the larger aircraft. For IFR conditions, boundaries were the same for both aircraft and about 50 percent less than those for VFR conditions.

Upsets as small as 7° in bank angle were considered hazardous at the lower altitudes for both flight conditions. Proximity to the ground was the primary reason for a hazardous rating. This was reflected in the reduction in the maximum bank angle at the hazard boundary and in the more consistent ratings as altitude was decreased.

APPENDIX A

MOTION LOGIC AND FREQUENCY RESPONSE OF FSAA

Motion Logic

The motion drive logic is designed to convert the calculated 6-DOF pilot station accelerations of the simulated aircraft into six velocity drive signals which move the simulator, within its physical limits, such that the combined effects of acceleration and gravity subject the pilot to forces that best approximate those that he would experience in flying the real aircraft. This "best approximation" is that which gives the best representation of those forces which provide the pilot with motion cues that can influence his control of the aircraft. The motion drive logic used is shown in figures 12 and 13.

The inputs to this system consist of the calculated pilot station accelerations ($\ddot{A}_{x,y,z}$ and $\ddot{A}_{p,q,r}$) and the position of the simulator ($A_{FU_{x,y,z}}$ and $A_{FU_{\phi,\theta,\psi}}$). The outputs are the required cab translational velocities and rotational rates ($\dot{A}_{SD_{x,y,z}}$ and $\dot{A}_{SD_{\phi,\theta,\psi}}$).

As shown in figures 12 and 13, the pilot station accelerations are passed through fourth-order washout filters which strongly attenuate the low-frequency components, while allowing the high-frequency components to pass virtually unchanged. If the low-frequency components of acceleration were passed unattenuated to the simulator drive system, they would quickly cause the simulator to move to its position limits. The motion cues associated with the low-frequency translational accelerations are recovered by rotating the cab so that gravity forces provide components of acceleration that roughly equal the calculated low-frequency translational forces. However, this cab rotation (residual tilt, fig. 13) must be accomplished at cab rotational accelerations undetectable to the pilot and can only be applied to compensate the forces in the X-Y plane.

The outputs from the residual tilt and rotational drive calculation ($\dot{A}_{CL_\ell}$ and $\dot{A}_{CN_i}$, fig. 13) usually contain some high-frequency rotational motion, due to the effects of gravity, which could produce false translational motion cues if left uncompensated. These spurious motion cues are removed by additional cab translational accelerations (fig. 12) such that the corresponding inertial forces cancel the unwanted gravitational forces. Any long-term components of the calculated translational velocities and rotational rates are compensated for by the addition of a first-order washout filter.

To ensure that the simulator drive commands result in the desired simulator translational and rotational displacements, a position error term is added to the velocity command to form the total translational and rotational drive signals. This position error correction consists simply of multiplying the difference in the actual and desired simulator positions by an appropriate gain and then adding this value to the desired simulator velocities and rates

to get the corrected simulator drive commands ($\dot{A}_{SD_{x,y,z}}$ and $\dot{A}_{SD_{\phi,\theta,\psi}}$). Appropriate limiting logic is included in the motion system to prevent the simulator from exceeding various acceleration, velocity, and position limits.

The motion program coefficients, gains, and limits are adjusted until the measured acceleration of the simulator cab matches as closely as possible the computed acceleration of the airplane, and the excursions of the simulator into its limits occurs only infrequently. The notation used herein, and the coefficients, gains, and limits used for this program are presented in tables 5 and 6.

Frequency Response

An all-digital, six-axis, frequency evaluation program (SAFE) has been developed to check the response characteristics of the simulator. This system drives all six axes simultaneously by a sum of sinusoids for approximately 1 min. With this known input and the measured position responses, calculations are made to determine each of the driving frequencies.

Bode plots of amplitude ratio and phase lag measured for each axis are presented in figure 14. Because the SAFE program assumes that each axis does not respond to commands to other axes, these Bode plots are for the FSAA without washout compensation.

A similar SAFE program is also available to determine the frequency response of the visual system. Bode plots of amplitude ratio and phase lag for the visual system are presented in figure 15.

APPENDIX B

PILOT RÉSUMÉS

Included in this section are brief résumés of the experience and qualifications of the pilots taking part in the simulation.

Pilot A
Position: Engineering Test Pilot, NASA/Ames
Flight Time: (hr)

Single Engine	5 850
Multiengine	2 100
Other (Helicopter)	300
Total	8 250

Misc: Airline Transport Rating

Pilot B
Position: Flight Test Pilot, FAA/NAFEC
Flight Time: (hr)

Single Engine	3 000
Multiengine	5 500
Other	500
Total	9 000

Misc: Airline Transport Rating

Pilot C
Position: Flight Test Pilot, FAA/NAFEC
Flight Time: (hr)

Single Engine	1 200
Multiengine	4 500
Other	2 500
Total	8 200

Misc: Airline Transport Rating

Pilot D
Position: Engineering Test Pilot, FAA/AWE-105
Flight Time: (hr)

Single Engine	3 000
Multiengine	8 500
Other	1 300
Total	12 800

Misc: Airline Transport Rating

Pilot E
Position: Flight Test Pilot, FAA/NAFEC
Flight Time: (hr)

Single Engine	3 500
Multiengine	7 000
Other	3 000
Total	13 500

Misc: Airline Transport Rating

Pilot F
Position: Flight Test Pilot, USAF/Wright-Patterson AFB
Flight Time: (hr)

Single Engine	327
Multiengine	2 159
Other	634
Total	3 120

Misc: USAF Test Pilot School Graduate

Pilot G
Position: Flight Test Pilot, USAF/Wright-Patterson AFB
Flight Time: (hr)

Single Engine	150
Multiengine	3 100
Other	150
Total	3 400

Misc: USAF Test Pilot School Graduate

Pilot H
Position: Engineering Test Pilot, DOT/Canada
Flight Time: (hr)

Single Engine	4 450
Multiengine	5 750
Other	1 300
Total	11 500

Misc: Airline Transport Rating

REFERENCES

1. Israel, D. R.: Air Traffic Control: Upgrading the Third Generation. Tech. Rev., vol. 77, no. 3, 1975, pp. 14-24.

2. Roberts, L.: On Wake Vortex Alleviation. Presented at the NASA/ University of Kansas Conference on The Future of Aeronautics, Oct. 23-24, 1974.

3. FAA Symposium on Turbulence, Washington, D. C., March 22-24, 1971.

4. McCormack, B. W.: Aircraft Wakes: A Survey of the Problem. Presented at the FAA Symposium on Turbulence, Washington D. C., March 22-24, 1971.

5. Kirkman, K. L.; Brown, C. E.; and Goodman, A.: Evaluation of Effectiveness of Various Devices for Attenuation of Trailing Vortices Based on Model Tests in a Large Towing Basin. NASA CR-2202, 1973.

6. Garodz, L. J.; Hanley, W. J.; and Miller, N. J.: Abbreviated Investigation of the Douglas DC-10 Airplane Vortex Wake Characteristics in Terminal Area Type Operations. FAA/NAFEC Project No. 214-741, 04X (Special Task No. FS-2-73), 1972.

7. Kurkowski, R. L.; Barber, M. R.; and Garodz, L. J.: Characteristics of Wake Vortex Generated by a Boeing-727 Jet Transport During Two-Segment and Normal ILS Approach Flight Paths. NASA TN D-8222, 1976.

8. Elson, B. M.: Reduction in Aircraft Separations Sought. Aviation Week and Space Technology, vol. 103, no. 4, July 28, 1975, pp. 48-51.

9. Sammonds, R. I.; and Stinnett, G. W., Jr.: Hazard Criteria for Wake Vortex Encounters. NASA TM X-62,473, 1975.

10. Johnson, W. A.; and Myers, T. T.: A Model for Human Pilot Behavior During Wake Vortex Encounter Upsets. FAA-RD-76-8, (STI TR-1035-5), 1976.

11. Jewell, W. F.; and Stapleford, R. L.: Mathematical Models Used to Simulate Aircraft Encounters with Wake Vortices. STI TR-1035-4 (DOT-FA73WA-3276-1), 1975.

12. Johnson, W. A.; and Rediess, H. A.: Study of Control System Effectiveness in Alleviating Vortex Wake Upsets. AIAA Paper 73-833, Aug. 1973.

TABLE 1.- MOTION LIMITS - FLIGHT SIMULATOR FOR ADVANCED AIRCRAFT

Motions generated	Displacement	Acceleration	Velocity
Roll	±36°	1.6 rad/s^2	0.5 rad/s
Pitch	±18°	1.6 rad/s^2	.5 rad/s
Yaw	±24°	1.6 rad/s^2	.5 rad/s
Vertical	±4 ft (±1.22 m)	12 ft/s^2 (3.66 m/s)	7 ft/s (2.13 m/s)
Longitudinal	±3 ft (±0.91 m)	8 ft/s^2 (2.44 m/s^2)	5 ft/s (1.52 m/s)
Lateral	±40 ft (±12.19 m)	10 ft/s^2 (3.05 m/s^2)	16 ft/s (4.88 m/s)

TABLE 2.- COCKPIT INSTRUMENTATION AND CONTROLS

Number	Item
1	Collins FD109G attitude indicator (ADI)
2	Airspeed indicator
3	Angle-of-attack indicator for Boeing 707/720 (AOA for Learjet is hidden behind wheel)
4	Collins FD109G horizontal situation indicator (HSI)
5	Mach meter
6	Normal acceleration indicator, g units
7	Turn and bank indicator
8	Aileron and stabilizer trim control
9	Sideslip indicator
10	Longitudinal acceleration indicator, g units
11	Flap position control
12	Control wheel
13	Control column
14	Rudder pedals
15	Throttle levers
16	Marker beacon
17	Radio altimeter
18	Stabilizer trim indicator
19	Flap position indicator
20	Engine instruments (EPR, N, EGT)
21	Visual scene
22	Rudder trim control
23	Instantaneous vertical speed indicator (IVSI)
24	Altimeter
25	Gear position indicator
26	Gear control lever

TABLE 3.- NUMERICAL VALUES OF ROLL AND PITCH TURBULENCE VARIABLES

j	A_j, deg		N_j		ω_j, rad/s	
	Aileron	Elevator	Aileron	Elevator	Aileron	Elevator
1	0.23363	0.09555	1	2	0.1571	0.3142
2	.72188	.25725	3	5	.4712	.7854
3	1.1813	.52185	8	11	1.257	1.728
4	2.0	2.4880	19	27	2.985	4.241
5	1.0	2.0	40	50	6.283	7.854
6	1.0	3.1105	65	75	10.21	11.78

TABLE 4.- ENCOUNTER CONDITIONS

$\psi^{\circ}_{W/V}$	$\theta^{\circ}_{W/V}$	Sense
±3	-3	
0	-3	
±3	-3	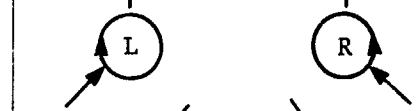
±3	3	
±7	-7	
0	-7	
±7	-7	
±7	0	
±10	-10	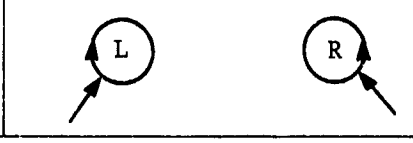

TABLE 5.- NOTATION FOR APPENDIX A

Axes systems	
Simulator	Orthogonal system of axes fixed in the simulator with translational rates $\dot{x}_s$, $\dot{y}_s$, and $\dot{z}_s$
Cab	Orthogonal system of axes fixed in the cab with translational accelerations $\ddot{x}_c$, $\ddot{y}_c$, and $\ddot{z}_c$ and angular accelerations $\dot{p}$, $\dot{q}$, and $\dot{r}$. Cab axes system related to simulator axes system by Euler angles ψ, θ, and ϕ.
Translational motion	
$\ddot{A}_{S_j}$	Simulated aircraft translational acceleration in the cab axes system
$\ddot{A}_{I_j}$	Filtered linear acceleration at the pilot station
$\ddot{A}_{CLH_j}$	Translational linear acceleration input to residual tilt calculations (output from high pass filters)
$\ddot{A}_{CN_k}$	Cab accelerations to compensate for gravity forces on cab due to angular position
$\dot{A}_{C_j}$	Desired cab translational velocities
$\dot{A}_{S_j}$	Desired simulator translational velocities prior to modification for position error
$\dot{A}_{SD_j}$	Simulator translational velocity drive commands
A_{FU_j}	Actual simulator translational position
A_{IC_j}	Initial position of simulator
Rotational motion	
$\ddot{A}_{S_i}$	Simulated aircraft angular acceleration in the cab axes system
$\ddot{A}_{I_i}$	Filtered rotational accelerations at the pilot station
$\ddot{A}_{CLL_k}$	Low-frequency translational accelerations to be represented by cab tilt

TABLE 5.- NOTATION FOR APPENDIX A — Continued

$\dot{A}_{N_i}$	Desired cab rotational velocities
$\dot{A}_{S_i}$	Desired simulator rotational velocities prior to modification for position error (sum of $\dot{A}_{CN_i}$ and $\dot{A}_{CL_i}$)
$\dot{A}_{CL_i}$	Rotational velocities ($\dot{\phi}$ and $\dot{\theta}$) for producing residual tilt
$\dot{A}_{CN_i}$	Desired simulator rotational velocities before compensation for residual tilt terms
$\dot{A}_{SD_i}$	Simulator rotational velocity drive commands
A_{S_i}	Desired simulator angular position including residual tilt (A_{CL_ℓ} and A_{CN_i})
A_{CL_ℓ}	Simulator angular position due to residual tilt
A_{CN_i}	Desired simulator angular position before compensation for residual tilt
A_{FU_i}	Actual simulator angular position
A_{IC_i}	Initial position of simulator
Transformations	
TM_{ji}	Euler angle transformation between cab and simulator axes
TM_{CL_ℓ}	Transformation to represent gravity in cab axes for computation of residual tilt to simulate low-frequency translational acceleration
TM_{LN_k}	Transformation to represent gravity in cab axes for computation of translational accelerations to compensate for force due to gravity
Gains	
$K1_j$	Washout gains for pilot station translational accelerations
$K1_i$	Washout gains for pilot station rotational accelerations

TABLE 5.- NOTATION FOR APPENDIX A — Concluded

$K5_j$	Position error feedback gain, translational axes
$K5_i$	Position error feedback gain, rotational axes
K_{N_k}	Gain in computation of translational accelerations to compensate for gravity force
K_{L_ℓ}	Gain in computation of residual tilt
K_{QP}	Residual tilt crossfeed gain (pitch to roll)
K_{RI_k}	Residual tilt gain for pilot station accelerations
Limits	
$\ddot{A}_{MA_j}$	Acceleration limits for pilot station translational accelerations
$\ddot{A}_{MA_i}$	Acceleration limits for pilot station rotational accelerations
$\dot{A}_{MA_j}$	Translational velocity limits
$\dot{A}_{MA_i}$	Rotational rate limits
$\dot{A}_{MA_\ell}$	Residual tilt rate limits
A_{MA_j}	Translational position limits
A_{MA_i}	Rotational position limits

TABLE 6.- MOTION PROGRAM COEFFICIENTS AND VALUES

	Symbol	Values
Washout filters		
Frequency	ω_{H1_x}, ω_{H2_x}	0.8, 0.8
	ω_{H1_y}, ω_{H2_y}	0.15, 0.15
	ω_{H1_z}, ω_{H2_z}	0.40, 0.40
	ω_{H1_p}, ω_{H2_p}	0.25, 0.25
	ω_{H1_q}, ω_{H2_q}	0.25, 0.25
	ω_{H1_r}, ω_{H2_r}	0.25, 0.25
Damping	ζ_{H1_x}, ζ_{H2_x}	1.414, 1.414
	ζ_{H1_y}, ζ_{H2_y}	1.414, 1.414
	ζ_{H1_z}, ζ_{H2_z}	1.414, 1.414
	ζ_{H1_p}, ζ_{H2_p}	1.414, 1.414
	ζ_{H1_q}, ζ_{H2_q}	1.414, 1.414
	ζ_{H1_r}, ζ_{H2_r}	1.414, 1.414
Gains	$K1_x$, $K1_y$, $K1_z$	0.4, 1.0, 0.7
	$K1_p$, $K1_q$, $K1_r$	0.5, 0.5, 0.5
Miscellaneous gains		
Position error feedback	$K5_x$, $K5_y$, $K5_z$	2.0, 0.1, 1.0
	$K5_p$, $K5_q$, $K5_r$	1.0, 1.0, 1.0
Translational due to rotation	K_{N_x}, K_{N_y}	0.0, 1.0
Residual tilt	K_{L_p}, K_{L_q}	4.0, 0.25

TABLE 6.- MOTION PROGRAM COEFFICIENTS AND VALUES — Concluded

	Symbol	Values
Limits	K_{QP}	1.0
	K_{RI_x}, K_{RI_y}	1.0, 1.0
	$\ddot{A}_{MA_x}$, $\ddot{A}_{MA_y}$, $\ddot{A}_{MA_z}$	8.0, 9.0, 11.0 ft/s^2
	$\ddot{A}_{MA_p}$, $\ddot{A}_{MA_q}$, $\ddot{A}_{MA_r}$	3.2, 1.6, 1.6 rad/s^2
	$\dot{A}_{MA_x}$, $\dot{A}_{MA_y}$, $\dot{A}_{MA_z}$	5.0, 16.0, 6.9 ft/s
	$\dot{A}_{MA_p}$, $\dot{A}_{MA_q}$, $\dot{A}_{MA_r}$	0.5, 0.5, 0.5 rad/s
	A_{MA_x}, A_{MA_y}, A_{MA_z}	2.8, 37.0, 3.9 ft
	A_{MA_p}, A_{MA_q}, A_{MA_r}	0.6283, 0.3141, 0.4185 rad

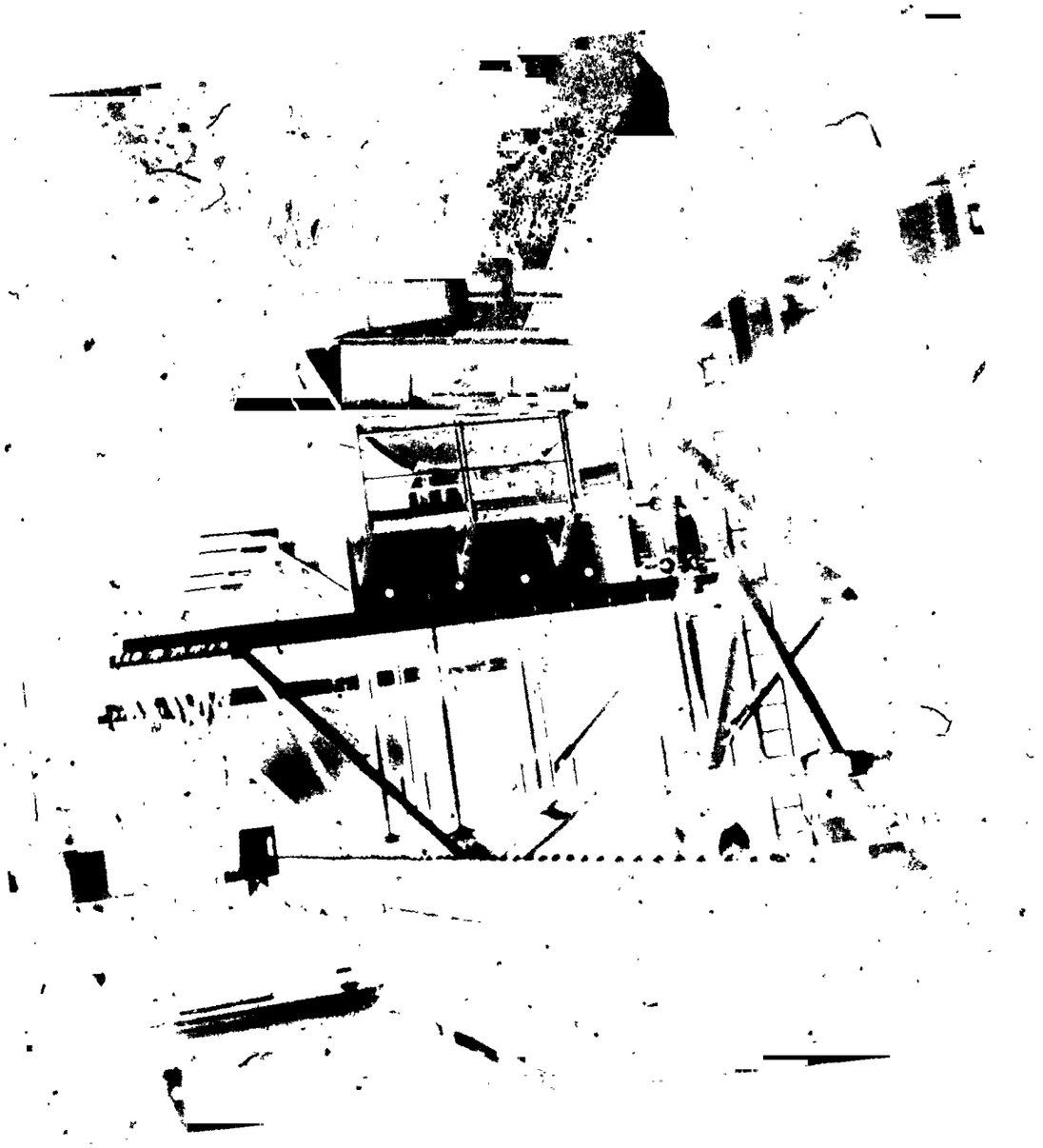

Figure 1.- Ames Flight Simulator for Advanced Aircraft (FSAA).

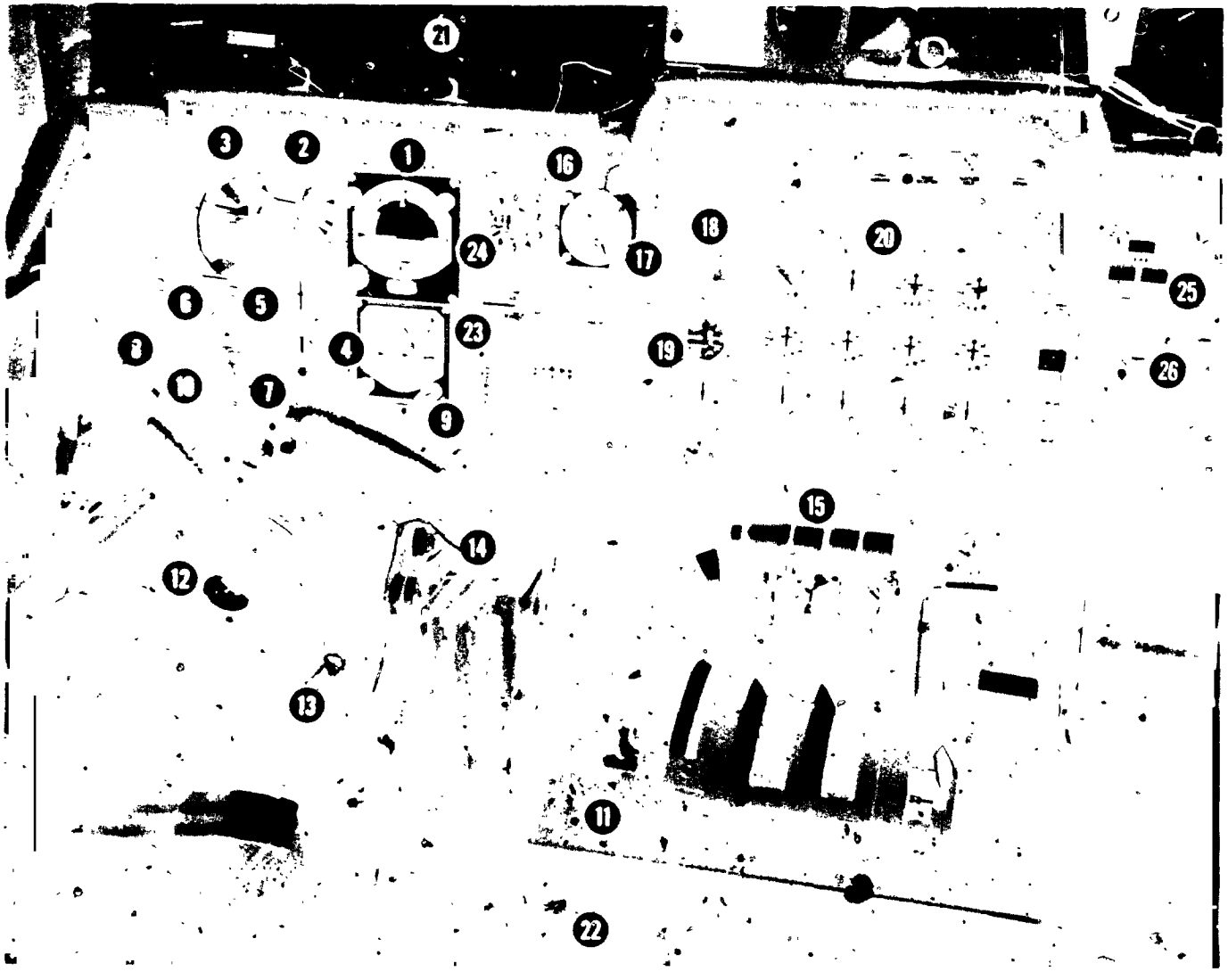

Figure 2.- Cockpit layout (see table 2 for identification of instruments and contro·).

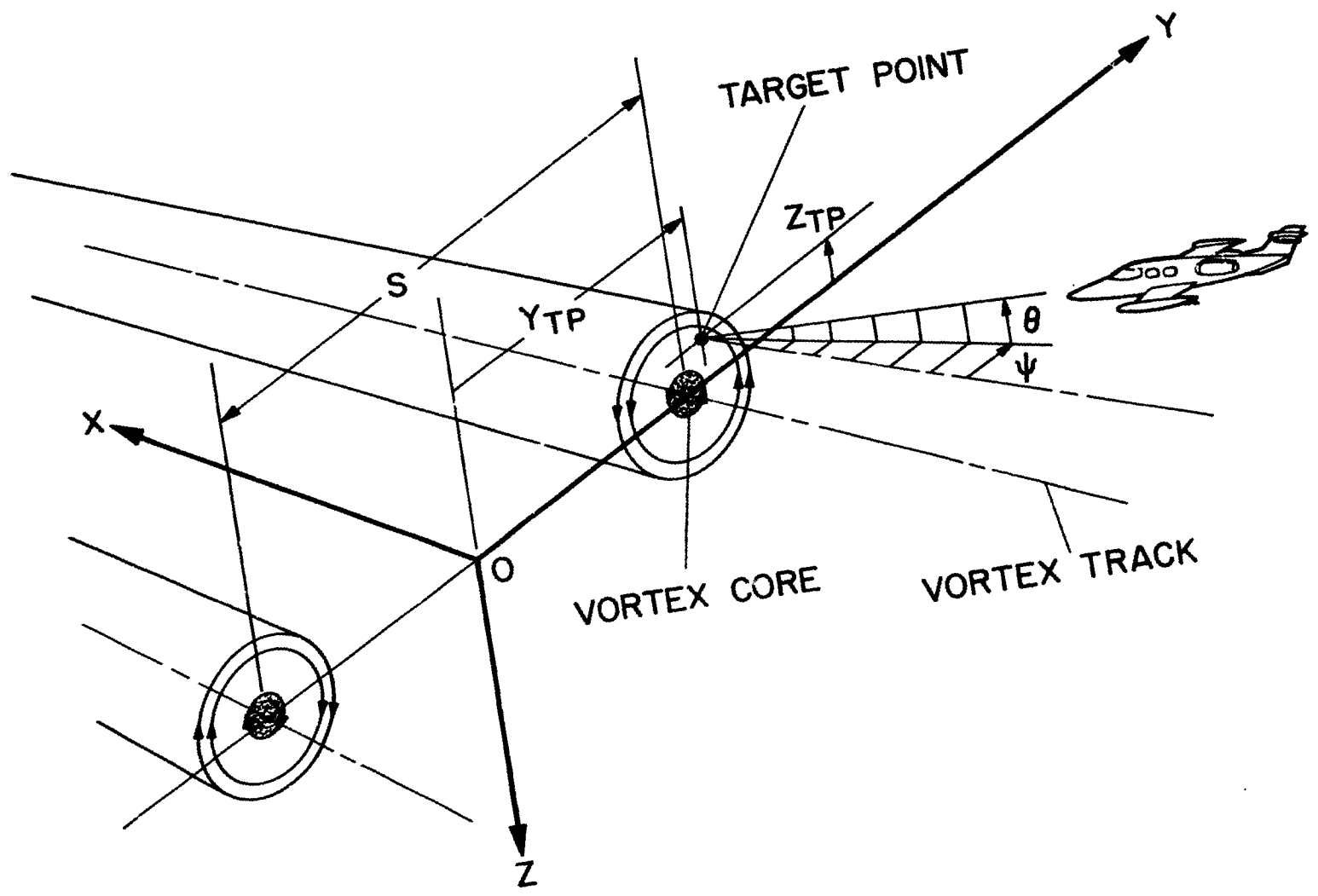

Figure 3.- Encounter geometry.

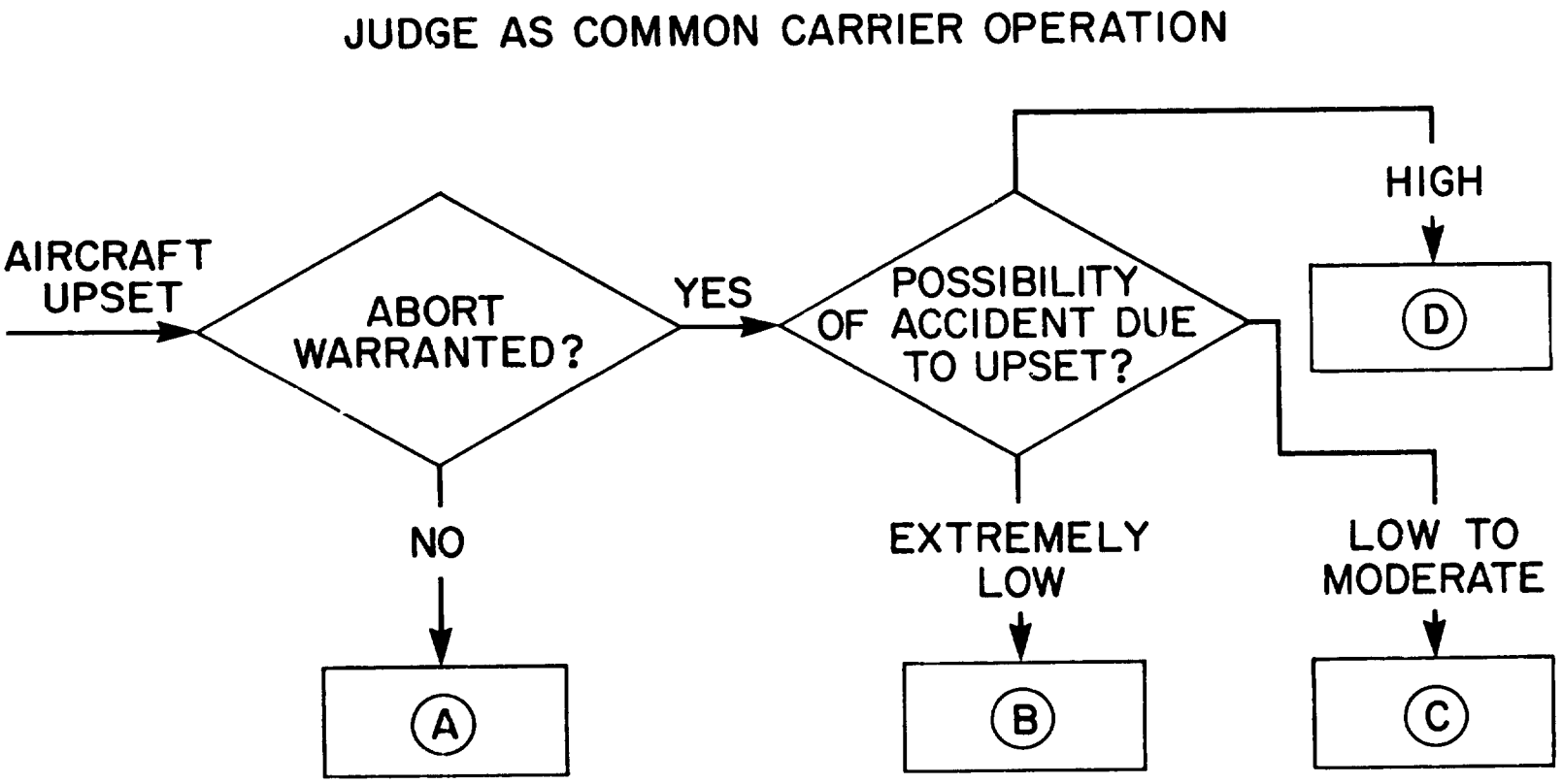

Figure 4.- Vortex encounter rating scale.

1. BRIEFLY DESCRIBE THE UPSET?

2. WAS THE UPSET REALISTIC?

3. COULD YOU DETECT WHETHER THE UPSET RESULTED FROM ATMOSPHERIC OR VORTEX TURBULENCE?

4. BRIEFLY DESCRIBE HOW THE UPSET WAS HANDLED?

5. DID YOU EXPERIENCE ANY DISORIENTATION?

6. PRIMARY REASON FOR PILOT RATING?

7. ANY OTHER COMMENTS?

Figure 5.- Pilot questionnaire.

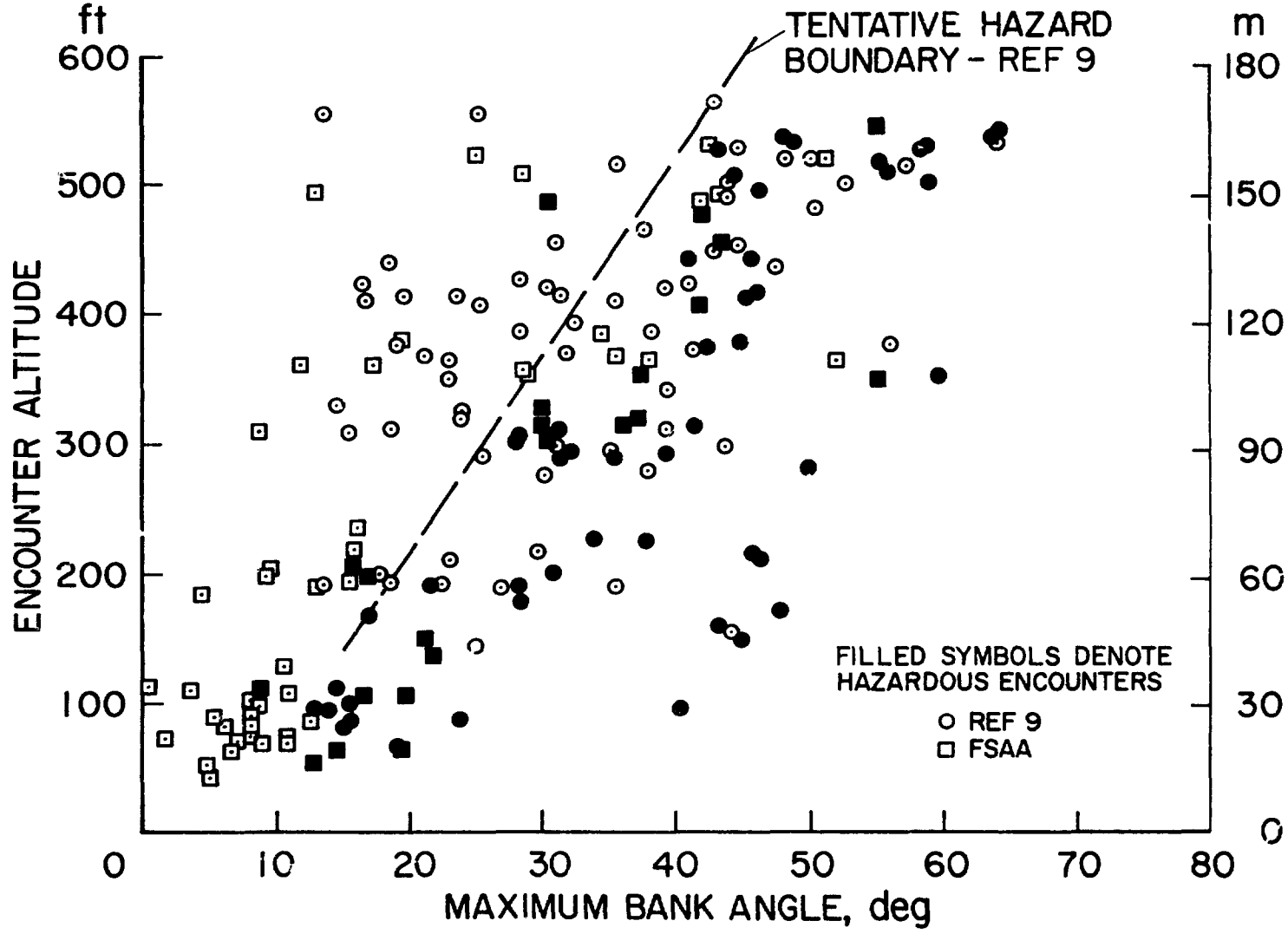

Figure 6.- Comparison of hazard boundary from two simulators.

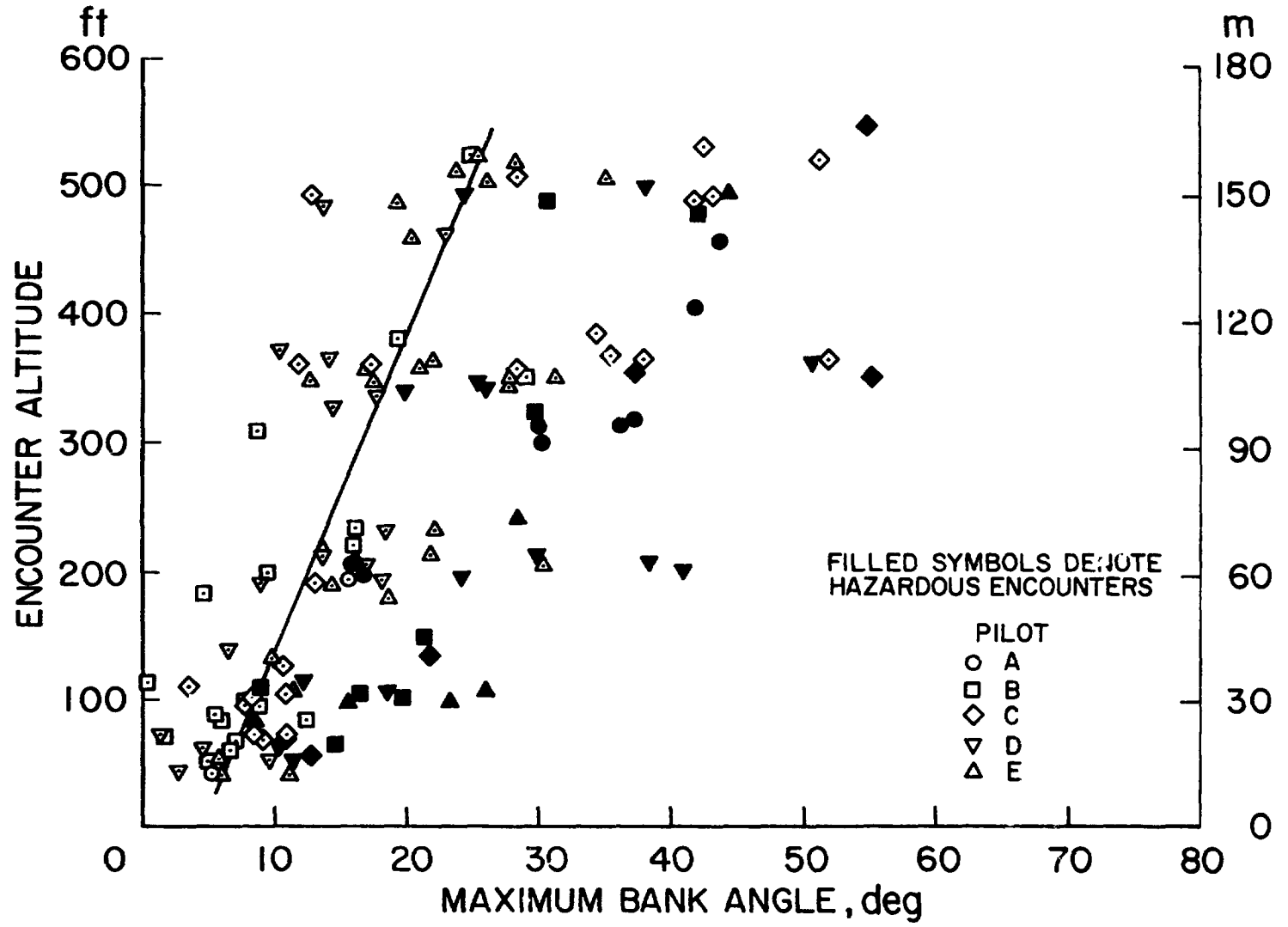

Figure 7.- Variation of encounter hazard with maximum bank angle and encounter altitude, Learjet/VFR.

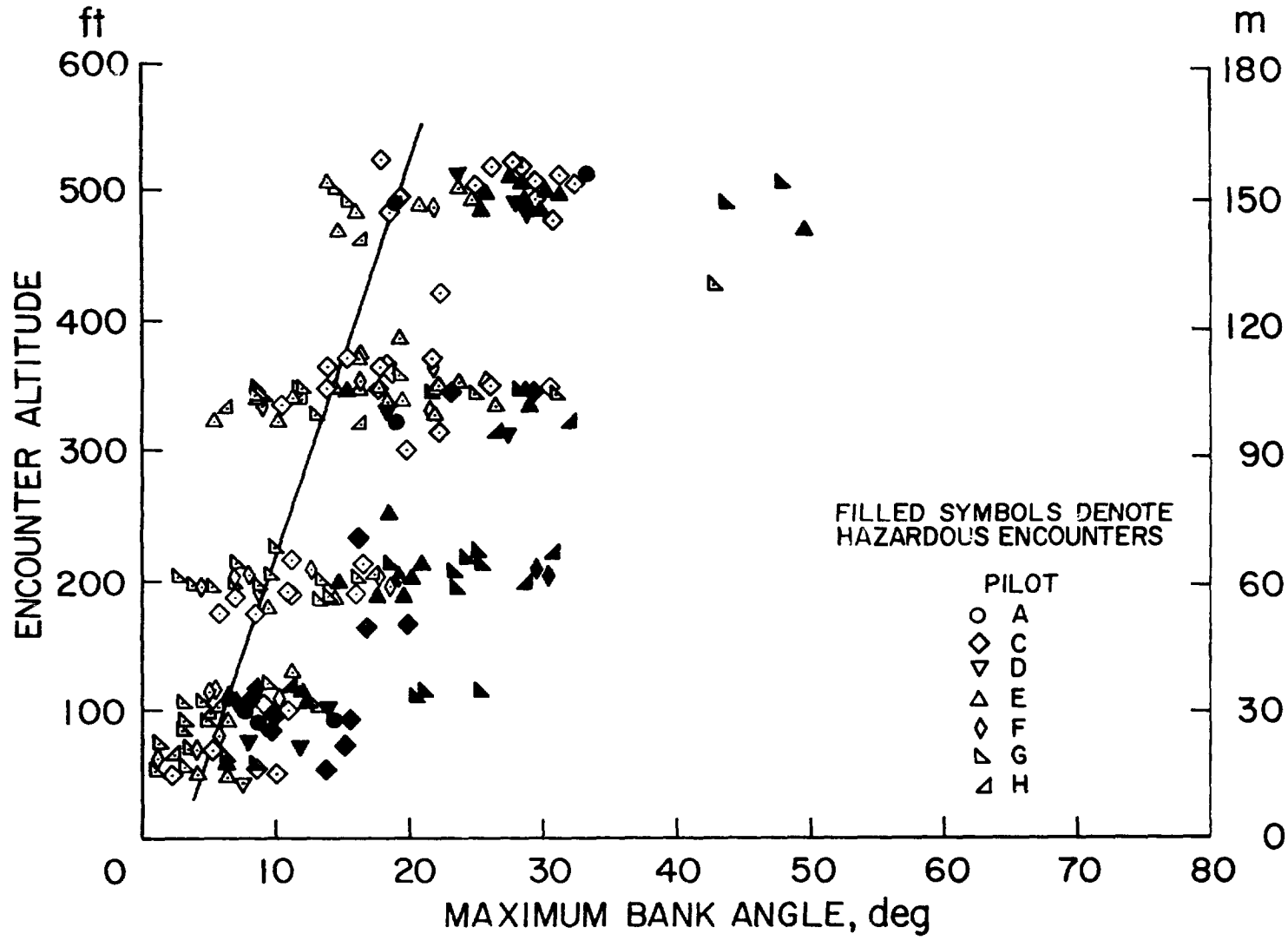

Figure 8.- Variation of encounter hazard with maximum bank angle and encounter altitude, Boeing 707/720/VFR.

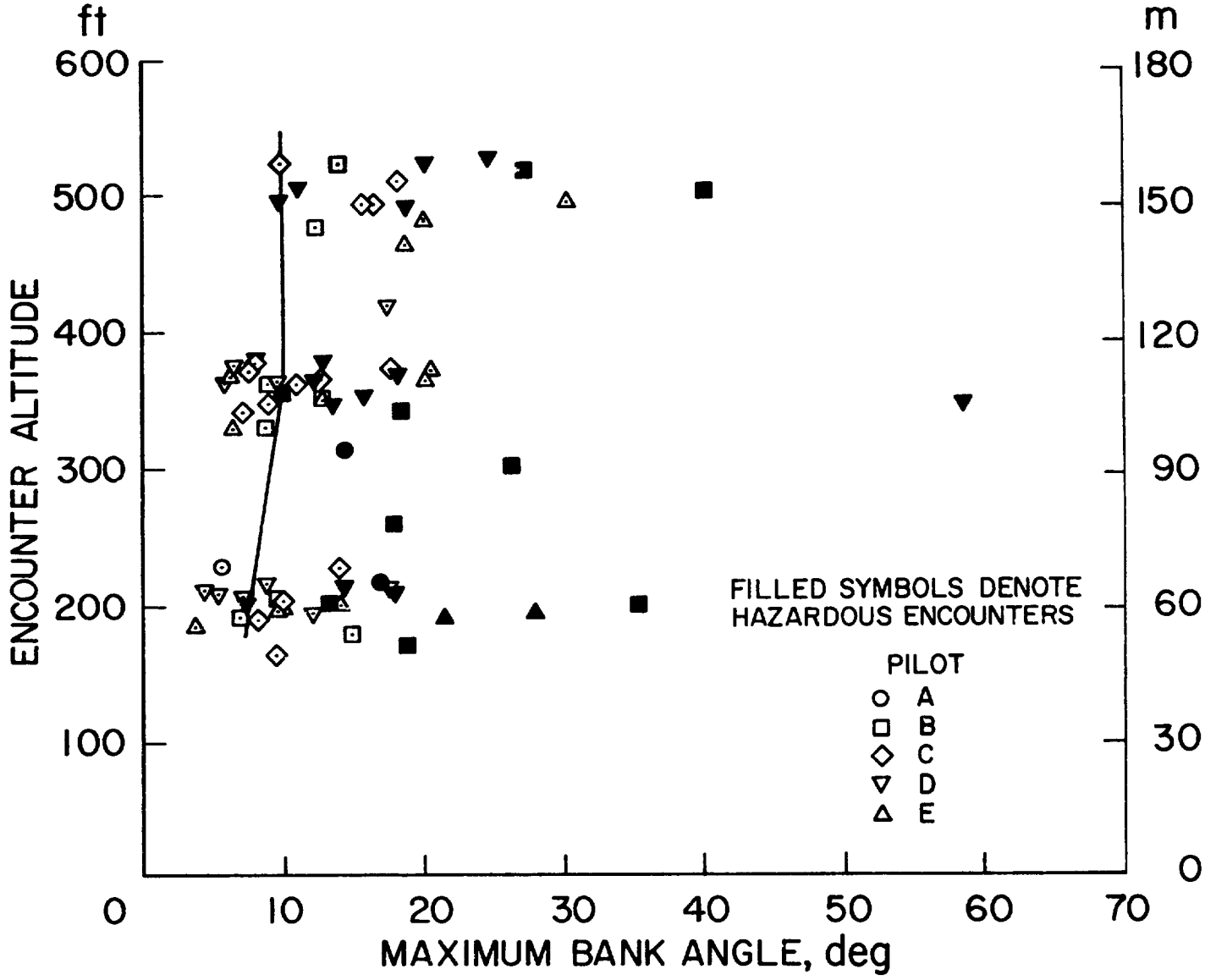

Figure 9.- Variation of encounter hazard with maximum bank angle and encounter altitude, Learjet/IFR.

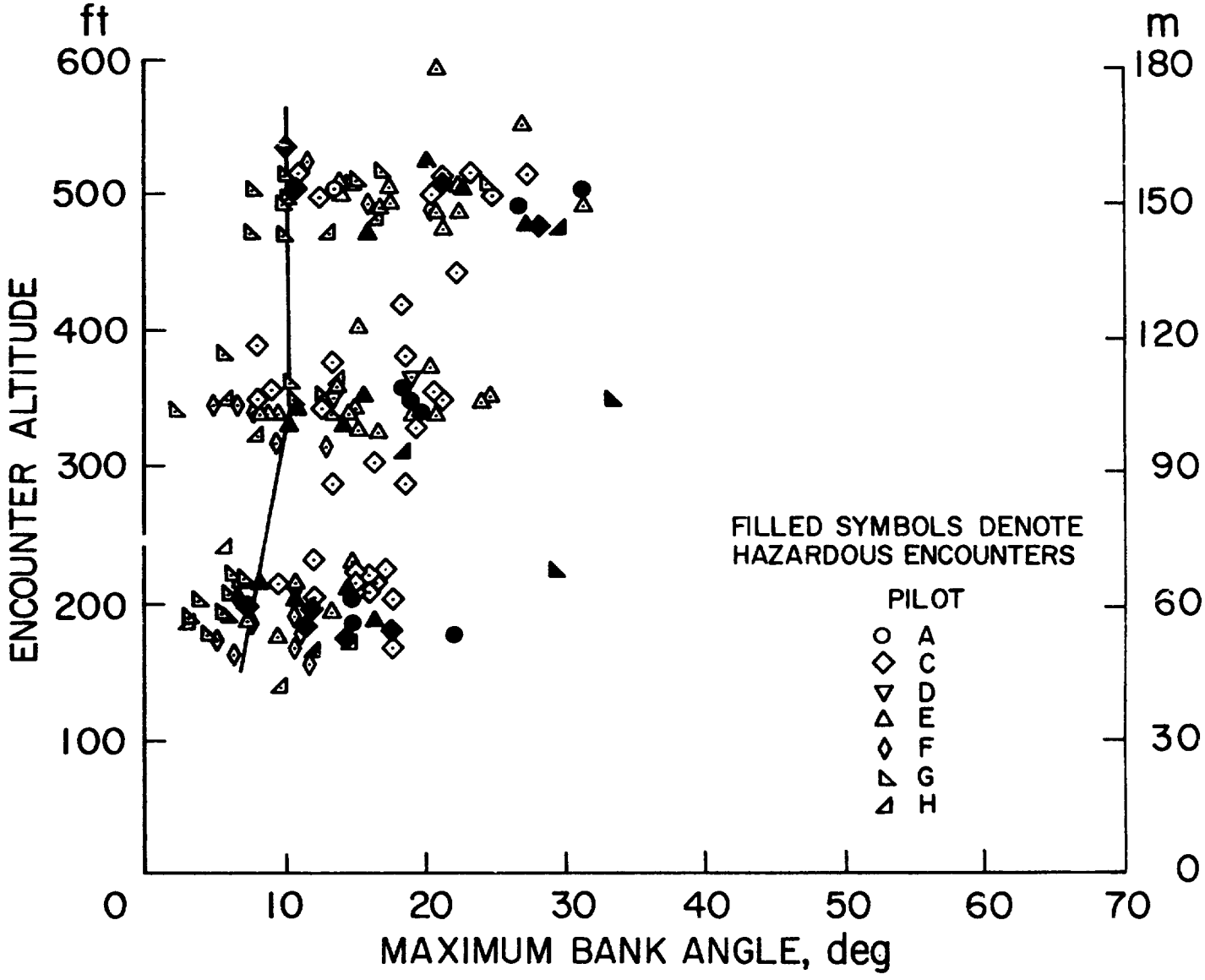

Figure 10.- Variation of encounter hazard with maximum bank angle and encounter altitude, Boeing 707/720/IFR.

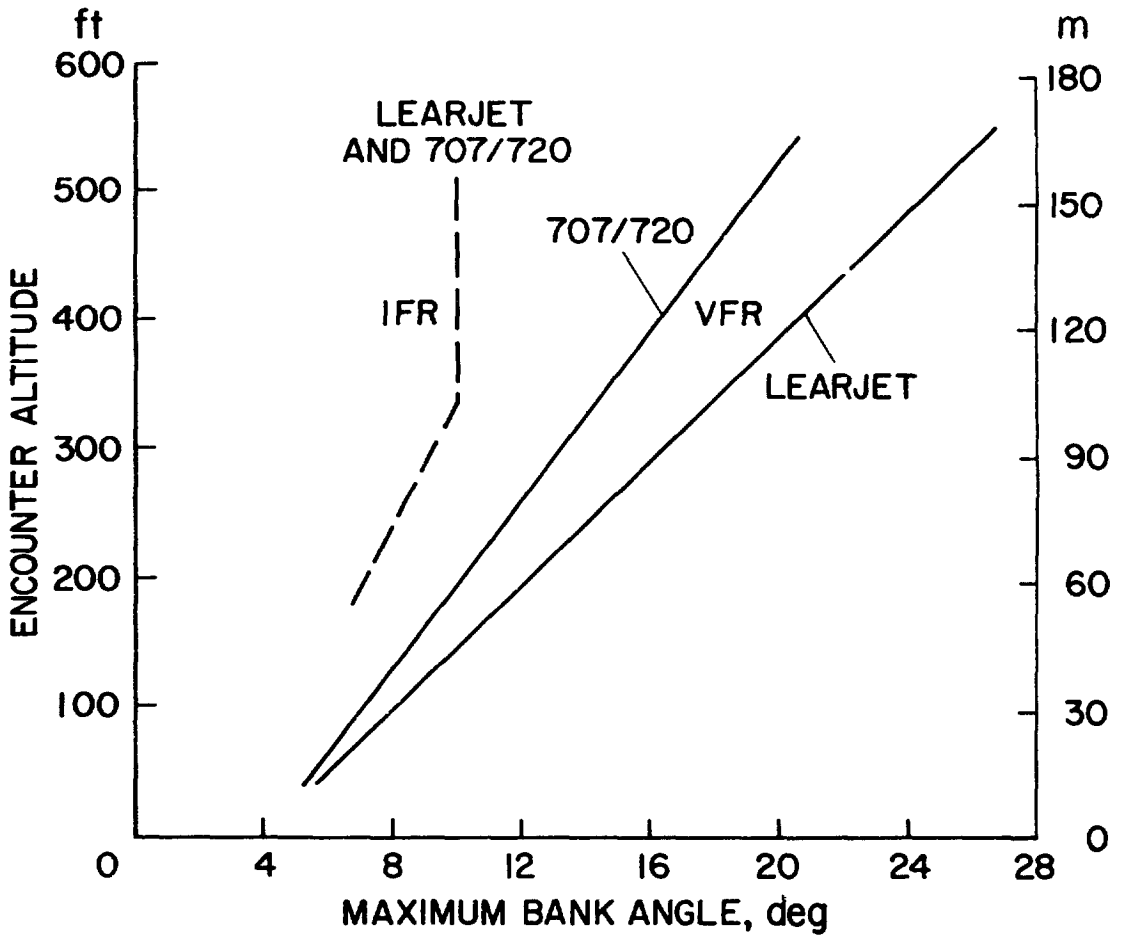

Figure 11.- Indicated hazard criteria for Learjet and Boeing 707/720 for both VFR and IFR flight conditions.

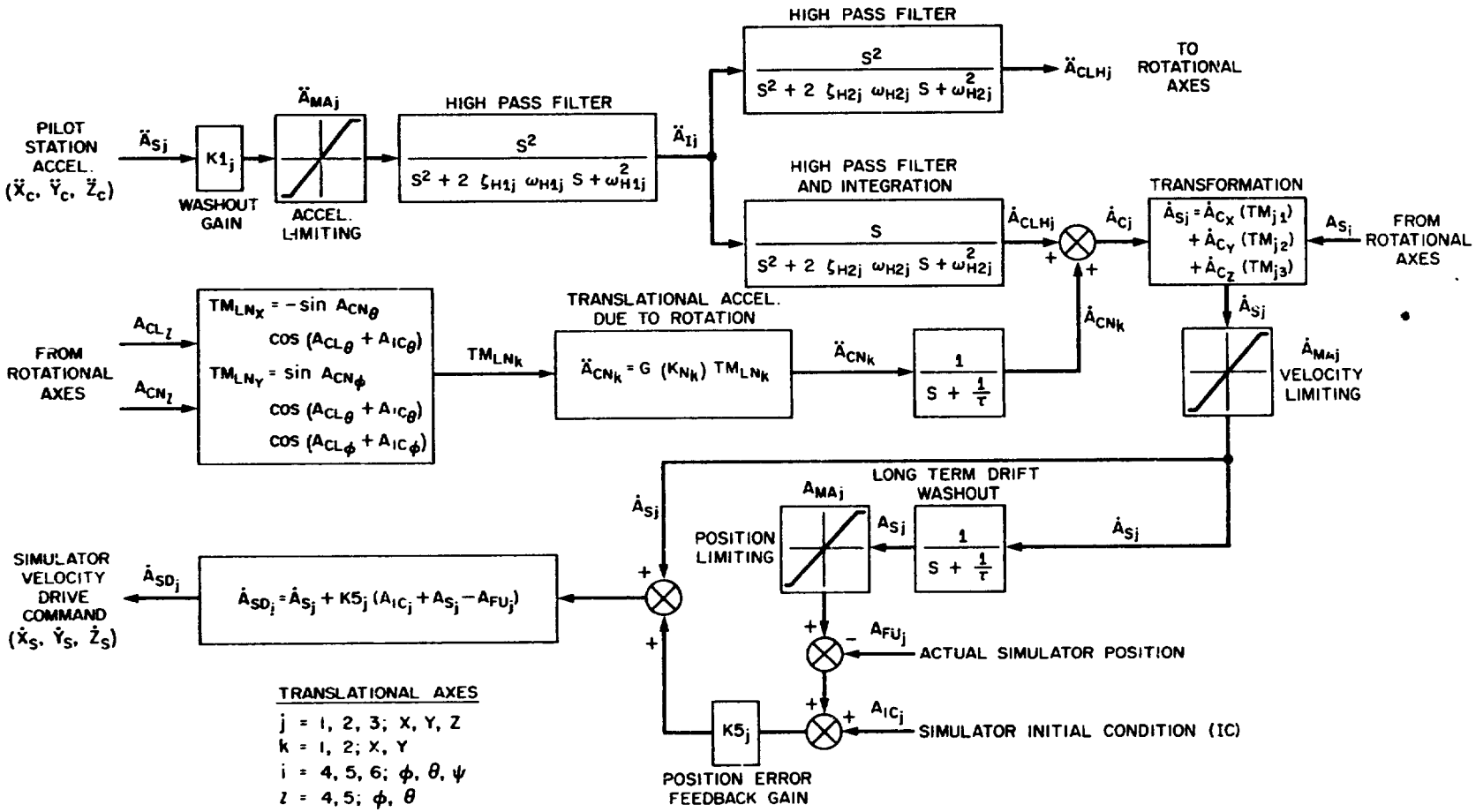

Figure 12.- Block diagram of translational axes motion washout system for the FSAA.

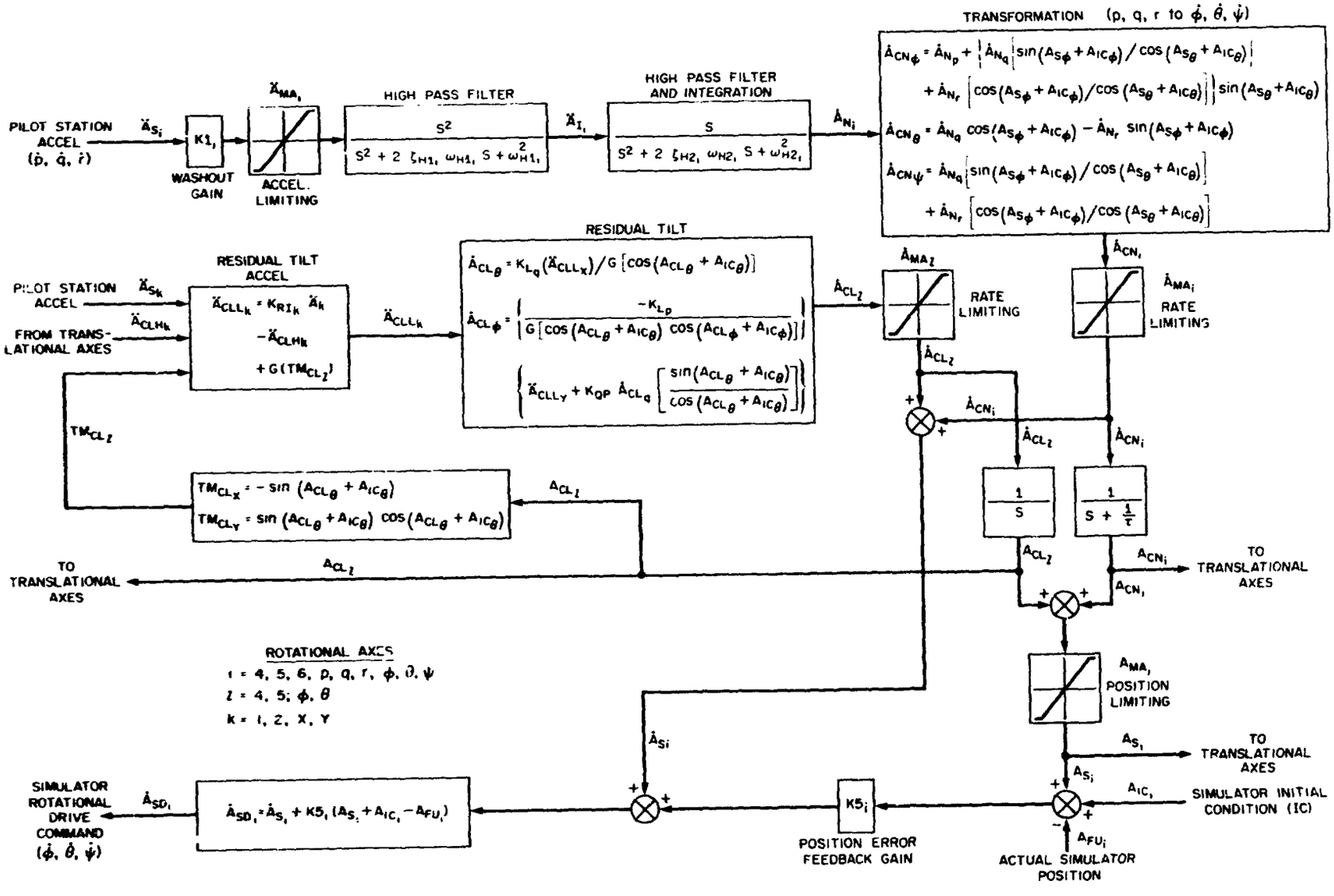

Figure 13.- Block diagram of rotational axes motion washout system for the FSAA.

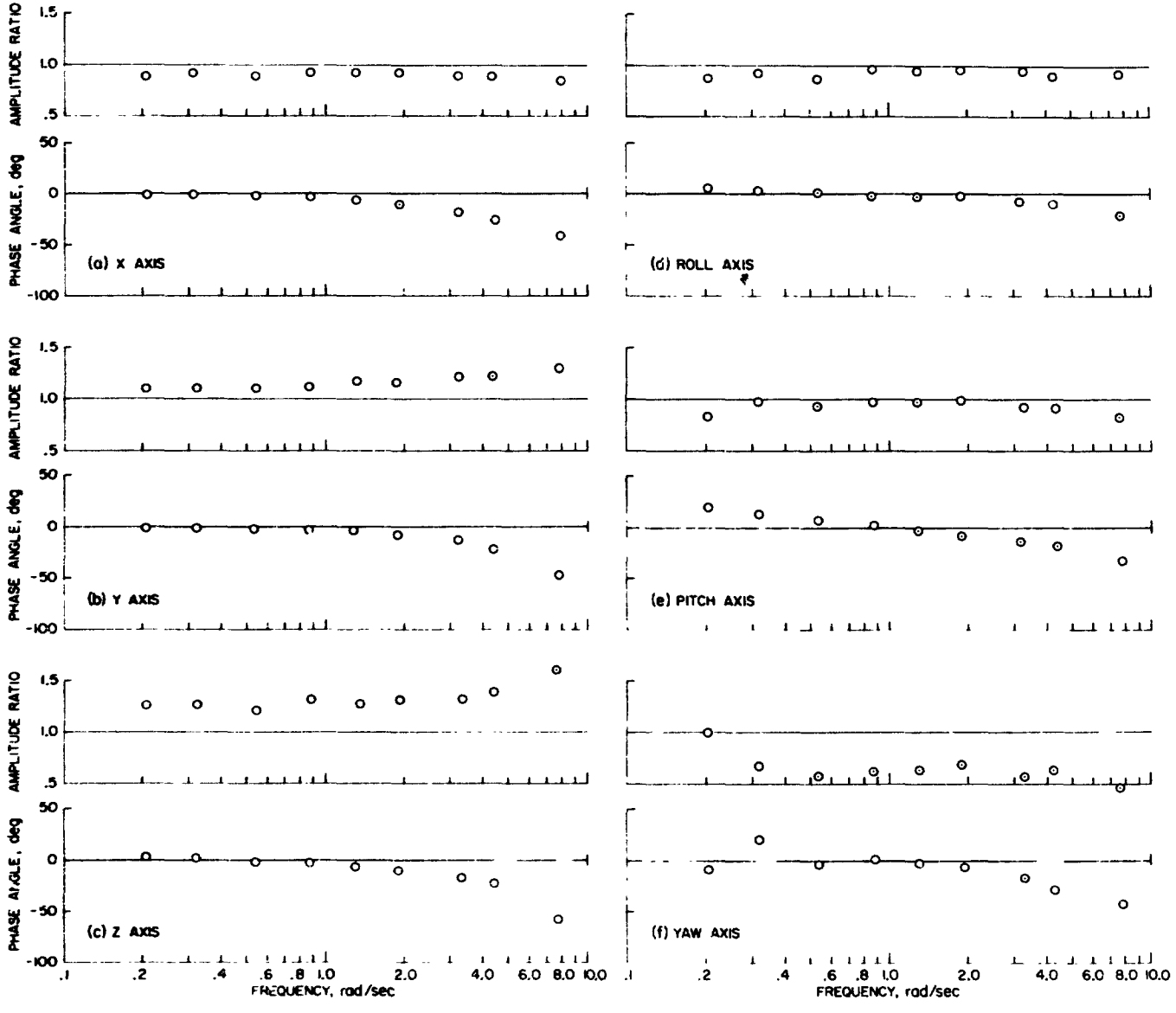

Figure 14.- Frequency response characteristics of the FSAA without washout.

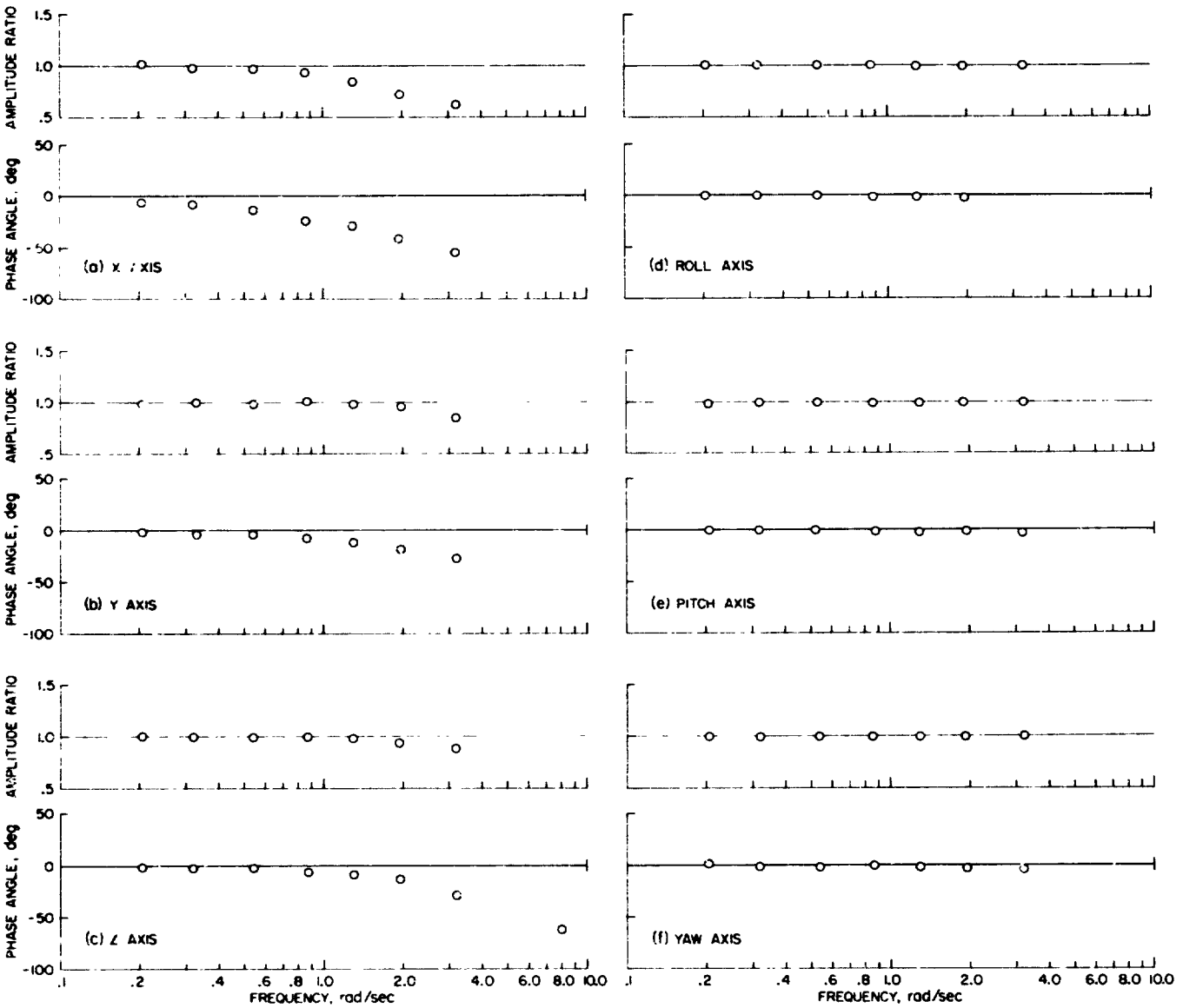

Figure 15.- Frequency response characteristics of the VFA 7 visual system.